Expected BGC Limitations

S. Udrea, P. Forck

GSI Helmholtzzentrum für Schwerionenforschung, Darmstadt, Germany

Outline

- Beam Induced Fluorescence (BIF) working principle and features
- N_2, Ne and Ar as working gases
- Image distortion due to electromagnetic fields
- Curtain thickness influence
- Possible show stoppers
- Conclusion

Beam Induced Fluorescence (BIF)

- Based upon the detection of photons emitted by residual or injected (low pressure) gas molecules
- Little influence on the beam
- Single pulse observation possible; e.g. ≈ 1 µs time resolution (depends on photon flux)
- Spatial resolution can be matched to application
- In case of low photon fluxes, commercial intensified cameras are available
- Compact installation, e.g. 25 cm for both planes

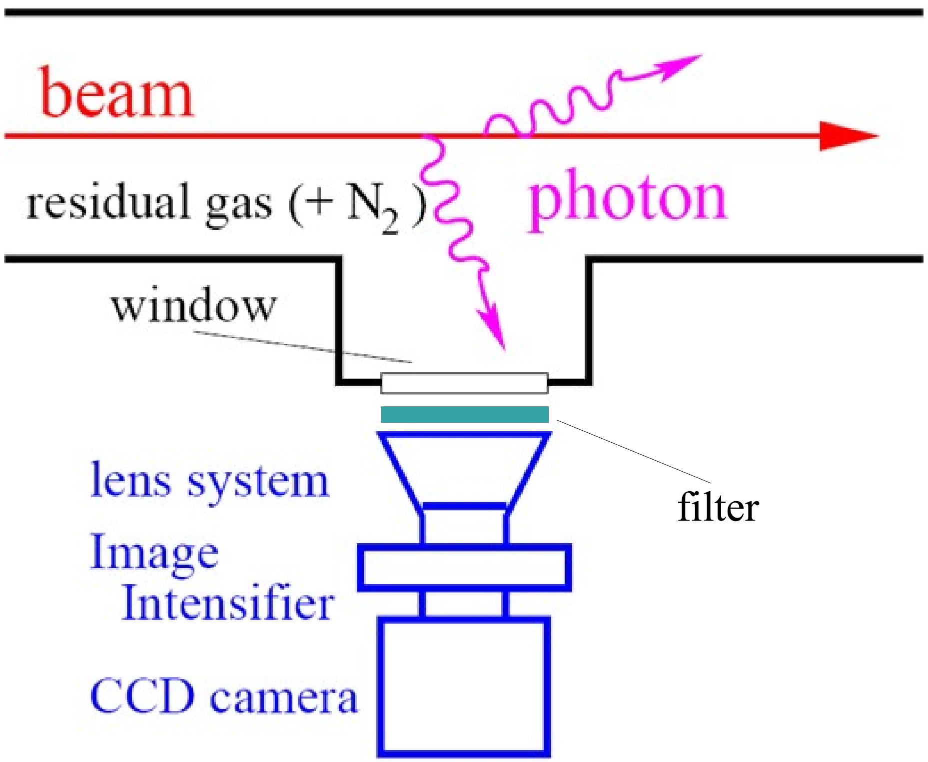

Fluorescence of different gases

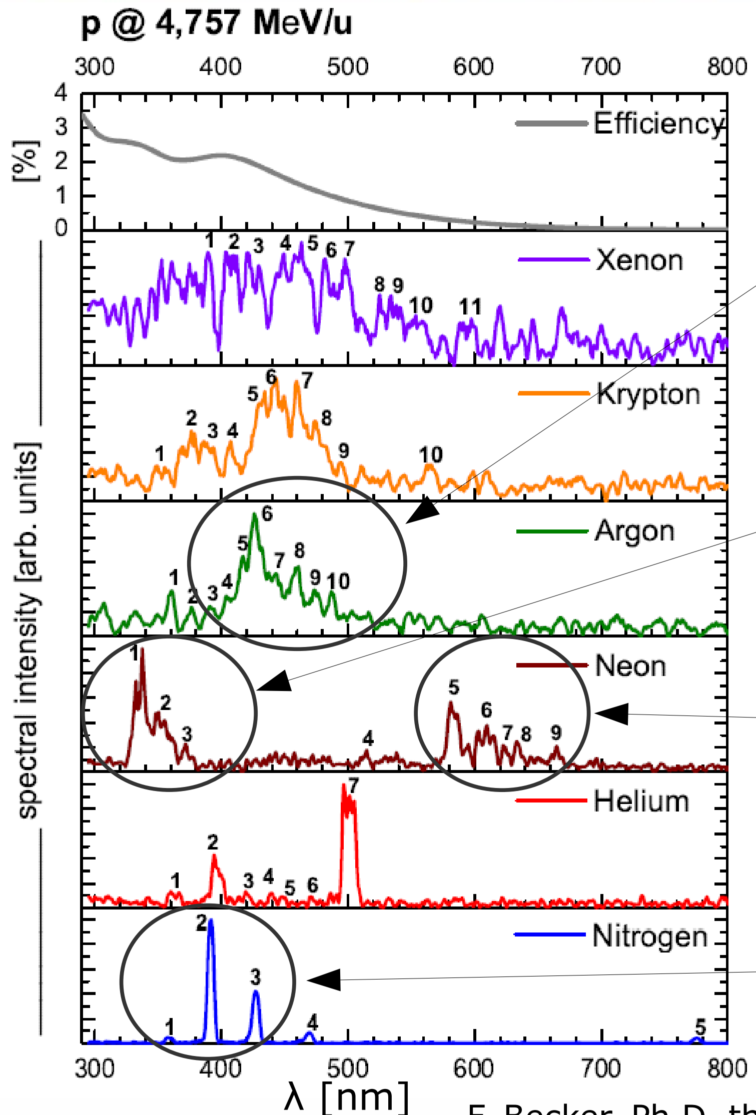

Strongest emission from Ar^+ blue/green lines mainly corresponding to different $[3s^2 3p^4(^3P)]4p \rightarrow 4s$ transitions with life times of 10-20 ns.

Several Ne^+ UV lines mainly corresponding to different $[2s^2 2p^4(^3P)]3p \rightarrow 3s$ transitions with life times below 10 ns.

Several Ne yellow/red lines mainly corresponding to different $[2s^2 2p^5(^2P)]3p \rightarrow 3s$ transitions with life times of about 20 ns.

The strong UV/blue lines correspond to the $B^2\Sigma_u^+ \rightarrow X^2\Sigma_g^+$ electronic transition band of N_2^+, life times are of about 60 ns.

F. Becker, Ph.D. thesis, T.U. Darmstadt, Germany, 2009

On cross sections and other details

emission* cross section ≠ excitation cross section

Emission cross sections are relevant for BIF diagnostics and may be affected by cascades – the upper level of the observed transition gets populated from higher excited levels – and pressure – attention has to be payed both to the working pressure and the pressure for which data is available. Moreover the experimental setup's geometry may play an important role.

Excitation cross sections are not directly relevant for BIF diagnostics. However, theoretical models usually target these cross sections, which may be used to estimate the emission cross sections by taking branching into account and an appropriate modeling of cascades and pressure effects.

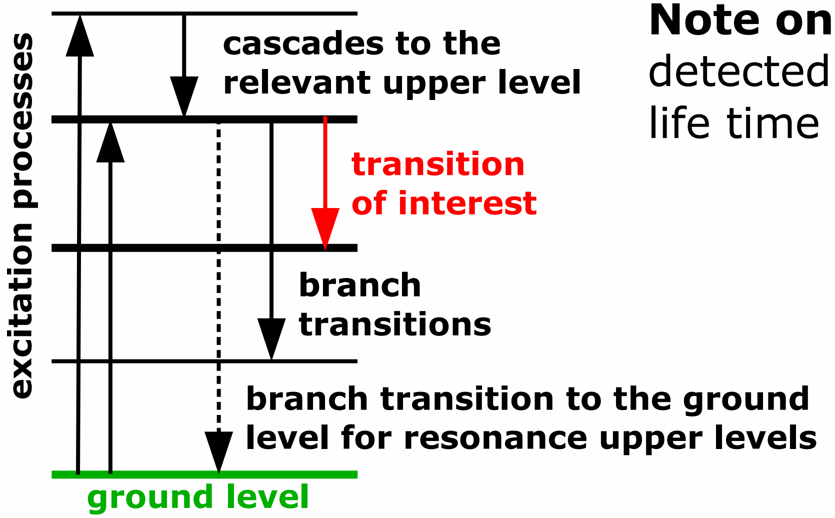

Note on branch transitions: If these can be detected too intensity increases and apparent life time decreases!

(*) also known as fluorescence cross section

N_2 as working gas: excitation and emission

$N_2 + p/e^- \rightarrow (N_2^+)^* + e^- + p/e^- \rightarrow N_2^+ + \gamma + e^- + p/e^-$

Leads to the electronic transition $B^2\Sigma_u^+ \rightarrow X^2\Sigma_g^+$ of the molecular ion with wavelengths around 391 nm, depending upon involved vibrational and rotational states. **Remark: cross section data available for a broad range of energies, up to p@450 GeV!**

υ' (upper level)	υ" (lower level)	λ [nm]	
1	0	358.2	
0	**0**	**391.4**	**strongest line**
0	1	427.8	

$N_2 + e^- \rightarrow (N_2)^* + e^- \rightarrow N_2 + \gamma + e^-$

Drives the electronic transition $C^3\Pi_u \rightarrow B^3\Pi_g$ of the neutral molecule with wavelengths around 337 nm. This process **cannot be initiated directly by protons** because it implies a spin flip mechanism: the upper $C^3\Pi_u$ state is a triplet one, while the ground state of N_2 is a singlet and total spin should stay preserved during excitation. **Remark: presently cross section data available just at low energies for e^- impact!**

υ'(upper level)	υ" (lower level)	λ [nm]	
1	0	315.9	
0	**0**	**337.1**	**strongest line**
0	1	357.7	

Ne as working gas: excitation and emission

$Ne + p/e^- \rightarrow (Ne^+)^* + e^- + p/e^- \rightarrow Ne^+ + \gamma + e^- + p/e^-$

Leads to several $[2s^2 2p^4(^3P)]3p \rightarrow 3s$ transitions of the Ne^+ ion with wavelengths between 300 and 400 nm. All transitions in the table below have lifetimes of about 6 ns. **Remark: No cross section data identified until now!**

$[2s^2 2p^4(^3P)]3p$	$[2s^2 2p^4(^3P)]3s$	λ [nm]	
J=7/2	J=5/2	319.9	
J=3/2	J=3/2	332.4	
J=1/2	**J=1/2**	**337.8**	**strongest line**

$Ne + p/e^- \rightarrow (Ne)^* + p/e^- \rightarrow Ne + \gamma + p/e^-$

Drives several $[2s^2 2p^5(^2P)]3p \rightarrow 3s$ transitions of Ne with wavelengths above 580 nm. Available data from the literature strongly suggests that the by far strongest line is due to the $2p_1 \rightarrow 1s_2$ (Paschen notation) transition at 585.4 nm. The upper level has a lifetime of about 15 ns. **Remark: Cross section data just at low energies until now! Cascades are expected to have little contribution to populating the $2p_1$ level.**

$[2s^2 2p^5(^2P)]3p$	$[2s^2 2p^5(^2P)]3s$	λ [nm]	
$2p_1$	**$1s_2$**	**585.4**	**strongest line**
$2p_3$	$1s_4$	607.4	
$2p_6$	$1s_5$	614.3	

Ar as working gas: excitation and emission

$Ar + p/e^- \rightarrow (Ar^+)^* + e^- + p/e^- \rightarrow Ar^+ + \gamma + e^- + p/e^-$

Leads to several $[3s^23p^4(^3P)]4p \rightarrow 4s$ transitions of the Ar^+ ion with wavelengths between 400 and 500 nm. The transitions in the table below have lifetimes of 10-20 ns. **Remark: presently cross section data available just up to 1keV for e^- impact! Upper levels are also populated by cascades but their contribution is small, approx. 5%.**

$[3s^23p^4(^3P)]4p$	$[2s^22p^4(^3P)]4s$	λ [nm]	
$^2P^o_{3/2}$	$^2P_{3/2}$	454.5	**significant branch**
$^2P^o_{3/2}$	$^2P_{1/2}$	**476.5**	**strongest line**

$Ar + p/e^- \rightarrow (Ar)^* + p/e^- \rightarrow Ar + \gamma + p/e^-$

Drives several $[3s^23p^5(^2P)]4p \rightarrow 4s$ transitions of Ar with the strongest at wavelengths above 700 nm. The upper levels from the table have lifetimes of 20-40 ns. **Remark: presently cross section data available just up to 1keV for e^- impact! No significant branching, cascades are not expected to lead to relevant distorsions.**

$[3s^23p^5(^2P)]4p$	$[3s^23p^5(^2P)]4s$	λ [nm]	
$2p_1$	$1s_2$	**750.4**	**strongest line**
$2p_5$	$1s_4$	751.5	

Image intensifier working principle

MCP based amplification module

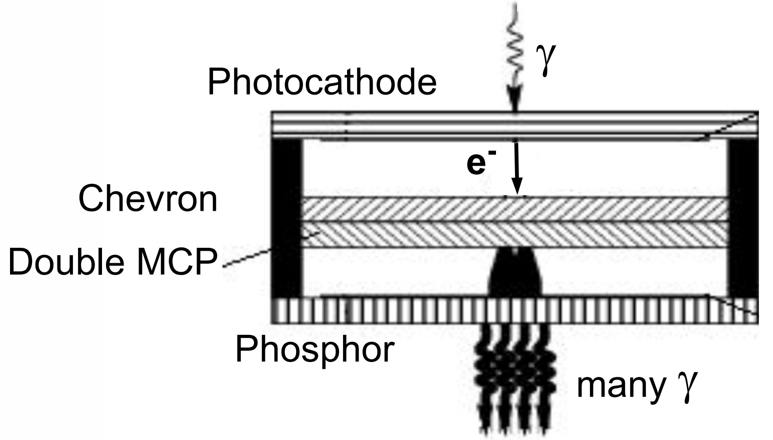

MCP structure

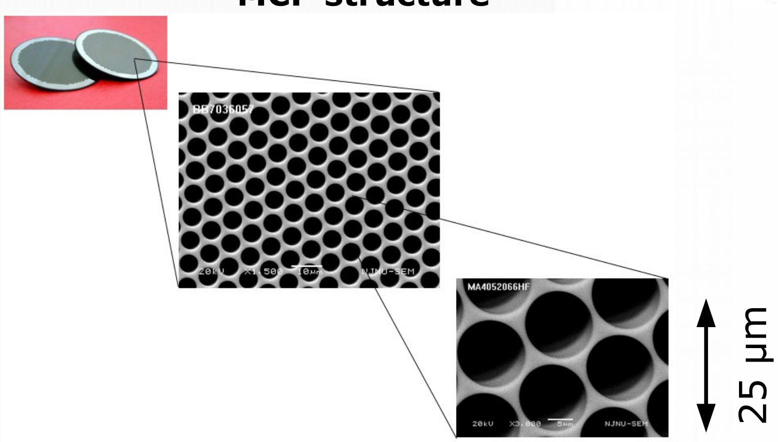

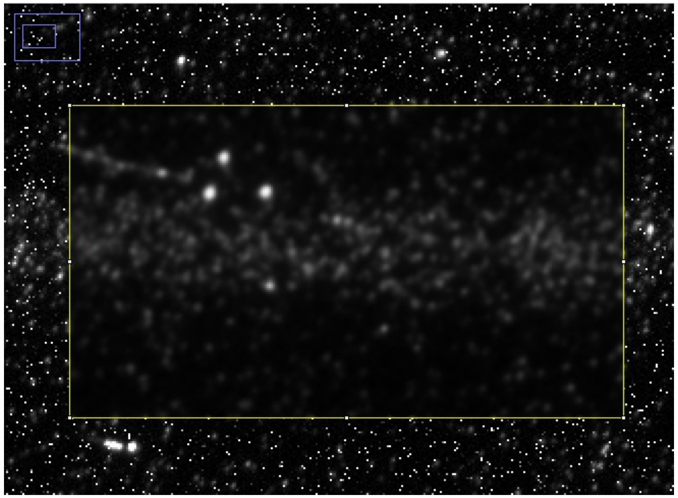

Image from $5 \cdot 10^8$, 300 MeV/u $^{238}U^{73+}$ ions in N_2, p= $5 \cdot 10^{-3}$ mbar.

Photocathode and camera

S20 photocathode:
- High quantum efficiency
- Sensitive for Ne yellow line
- Medium dark counts
- Availability

⇒ UV enhanced S20 chosen

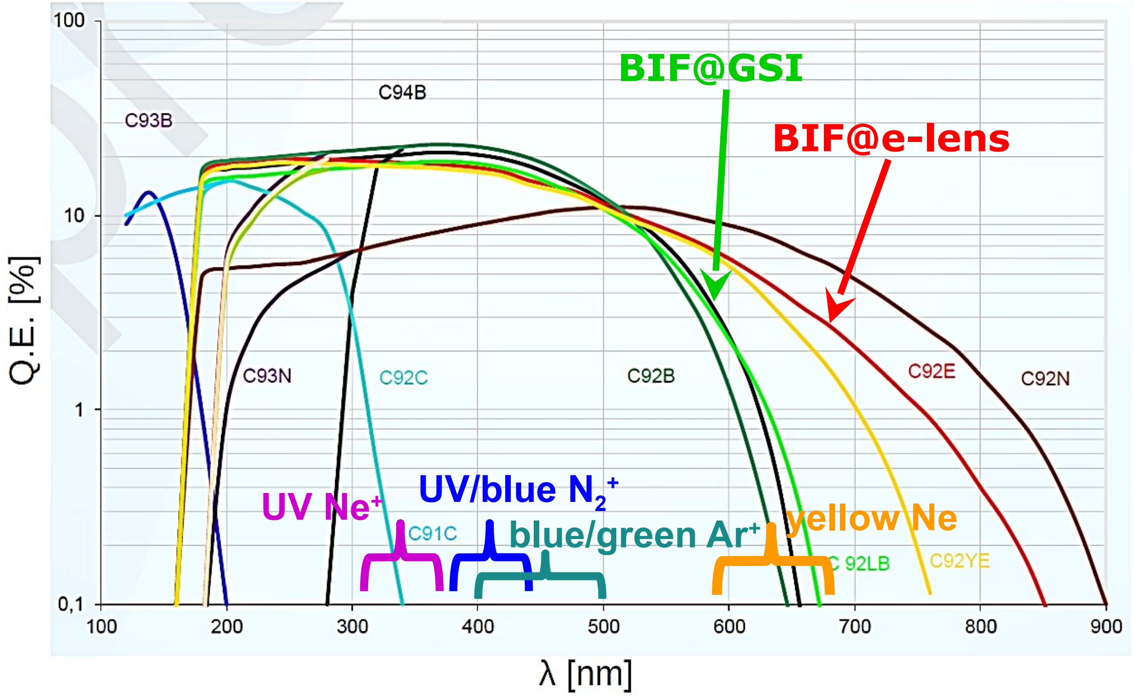

Image intensifier:
- double MCP for single photon counting; 10^6 amplification

Camera:
- Simple CMOS
- Coupling to CMOS by relay optics for easy maintenance

	Designation	Material	Peak Q.E. [%]	Dark counts [1/s/cm²]
BIF@e-lens	C92E	S20	20	600
BIF@GSI	C92LB	Low noise bialkali	20	15
	C92B, C93B, C94B	Bialkali	20	60
	C92N, C93N	S25	10	3000
	C92YE	Yellow enhanced	20	60

UV enhanced S20 spectral response

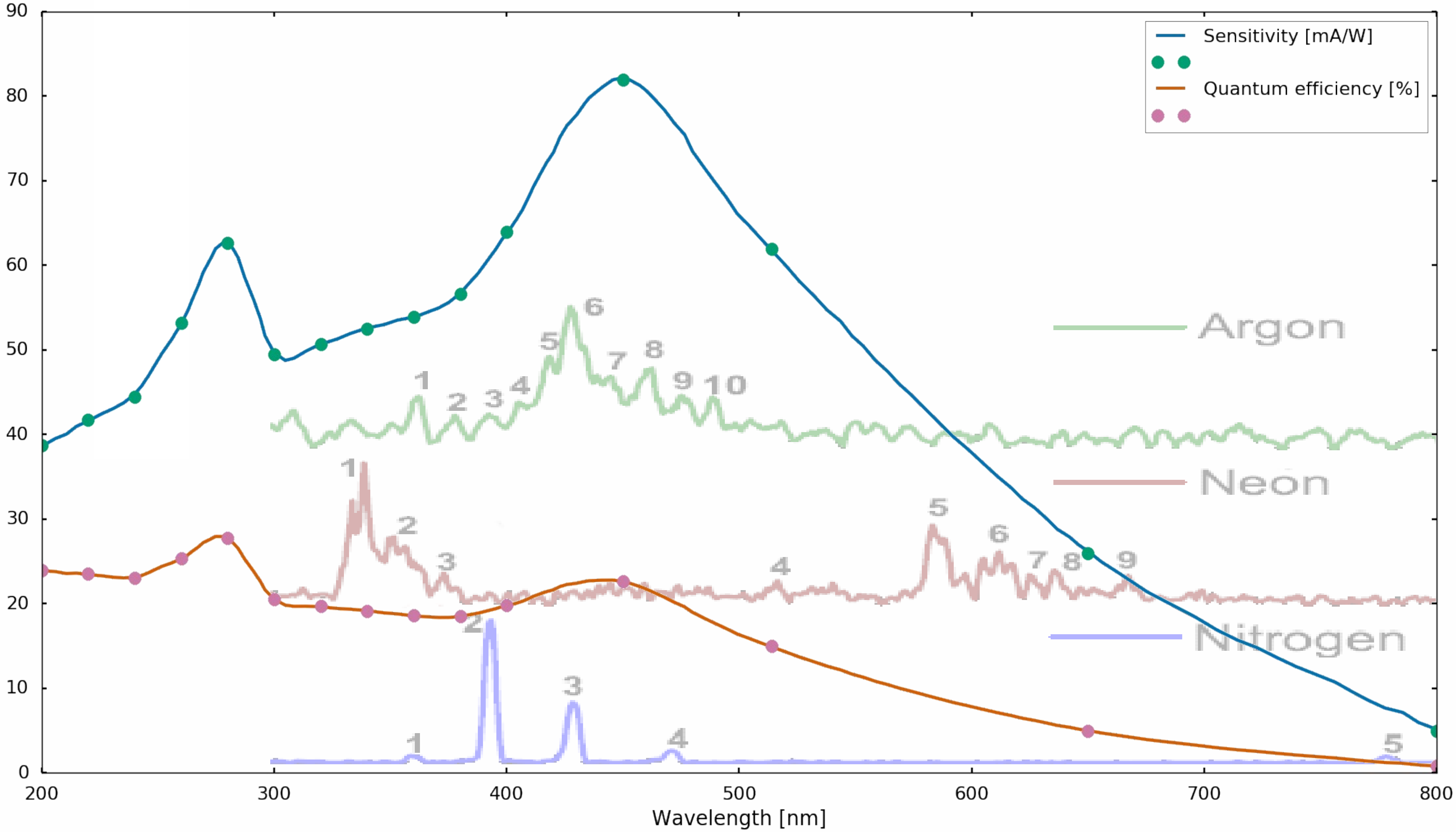

Based on data delivered by the manufacturer

Photon rate estimations

$$N_\gamma = \sigma \cdot \frac{I \cdot \Delta t}{e} \cdot n \cdot d \cdot \frac{\Omega}{4\pi} \cdot T \cdot T_f \cdot \eta_{pc} \cdot \eta_{MCP}$$

n = 2.5 · 10^{10} cm^{-3} (Still not there!)
d = 5 · 10^{-2} cm
Ω = **40π · 10^{-4} sr** (Scheimpflug!?)
T = 85%
T_f = 80%
η_{MCP} = 75%

N_γ = average number of photons detected during time Δt
σ = cross section of the photon generation process
I = electron or proton current (electrical)
e = elementary charge
n = gas density
d = distance traveled through gas (curtain thickness)
Ω = solid angle of the optics
T = transmittance of the optical system
T_f = transmittance of the optical filter
η_{pc} = quatum efficiency of the photocathode
η_{MCP} = detection efficiency of the MCP

Projectile	Emitter	λ [nm]	σ [cm^2]	I [A]	η_{pc}	N_γ [s^{-1}]	1/N_γ [s]
electron	N_2^+	391.4	$9.1\cdot10^{-19}$	5	0.19	$3.4\cdot10^{6}$	$2.9\cdot10^{-7}$
proton	N_2^+	391.4	$3.7\cdot10^{-20}$	1	0.19	$2.8\cdot10^{4}$	$3.6\cdot10^{-5}$
electron	Ne	585.4	$1.4\cdot10^{-20}$	5	0.09	$2.5\cdot10^{4}$	$4.0\cdot10^{-5}$
proton	Ne	585.4	$4.7\cdot10^{-22}$	1	0.09	$1.7\cdot10^{2}$	$5.9\cdot10^{-3}$
electron	Ar	750.4 & 751.5	$7.4\cdot10^{-20}$	5	0.02	$2.9\cdot10^{4}$	$3.4\cdot10^{-5}$
proton	Ar	750.4 & 751.5	$3.3\cdot10^{-21}$	1	0.02	$2.6\cdot10^{2}$	$3.8\cdot10^{-3}$
electron	Ar^+	454.5 & 476.5	$9.9\cdot10^{-21}$	5	0.20	$4.0\cdot10^{4}$	$2.5\cdot10^{-5}$
proton	Ar^+	454.5 & 476.5	$1.7\cdot10^{-21}$	1	0.20	$1.4\cdot10^{3}$	$7.4\cdot10^{-4}$

NEW

Working gases overview

	N_2	Ne	Ar
General remarks	Fluorescence almost exclusively due to N_2^+ at λ around 391 nm. Highest photon yield.	Strong fluorescence due to Ne at λ > 580 nm relatively strong emission due to Ne^+.	Strong Ar lines at λ > 700 nm, relatively strong Ar^+ lines for 400 < λ < 500 nm.
Life times (τ)	The relevant transition of N_2^+ has $\tau \approx 60$ ns. Cascades seem to play no role. No branching.	The relevant Ne^+ transitions have $\tau \leq 10$ ns, unknown cascade influence. The $2p_1$ Ne level has $\tau \approx 15$ ns, negligible branching and cascade influence.	Relevant Ar^+ transitions have $10 < \tau \leq 20$ ns, little cascade influence, branching can be advantageous(*). Ar lines have $20 \leq \tau \leq 40$ ns, cascades are not expected to significantly influence image quality.
Mass	28 u	20 u	40 u
τ^2/m	129 ns²/u	≤ 5 ns²/u, if no cascades!	(*)$2 \leq \tau \leq 10$ ns²/u
Exp. data availability for σ	Up to 1 keV for e^-, up to 450 GeV for p.	Ne: up to 1 keV for e^-, up to 1 MeV for p. Ne^+: no data identified yet.	Ar: up to 1 keV for e^-, none for p. Ar^+: up to 1 keV for e^-, none for p.
γ-cathode efficiency	Good for the strongest N_2^+ lines.	Poor for main Ne lines, good for Ne^+ lines.	Very poor for main Ar lines, good for Ar^+ lines.
e.m. fields influence	Relatively strong distortion expected due to large τ^2/m	None for Ne, relatively low distortion expected for Ne^+ because of low τ^2/m	None for Ar, relatively low distortion expected for Ar^+ because of low τ^2/m
Integration time	Very low for e^-, low for p, as estimated for the N_2^+ 391.4 nm line.	Low for e^-, large for p, as estimated for the Ne 585.4 nm line.	Lower than for Ne but large as compared to N_2^+. Integration over 400 < λ < 500 nm may be useful!

Simulations of expected images for N_2^+, Ne^+ and Ar^+

Simulations performed with the **virtual-ipm** code
pypi.org/project/virtual-ipm

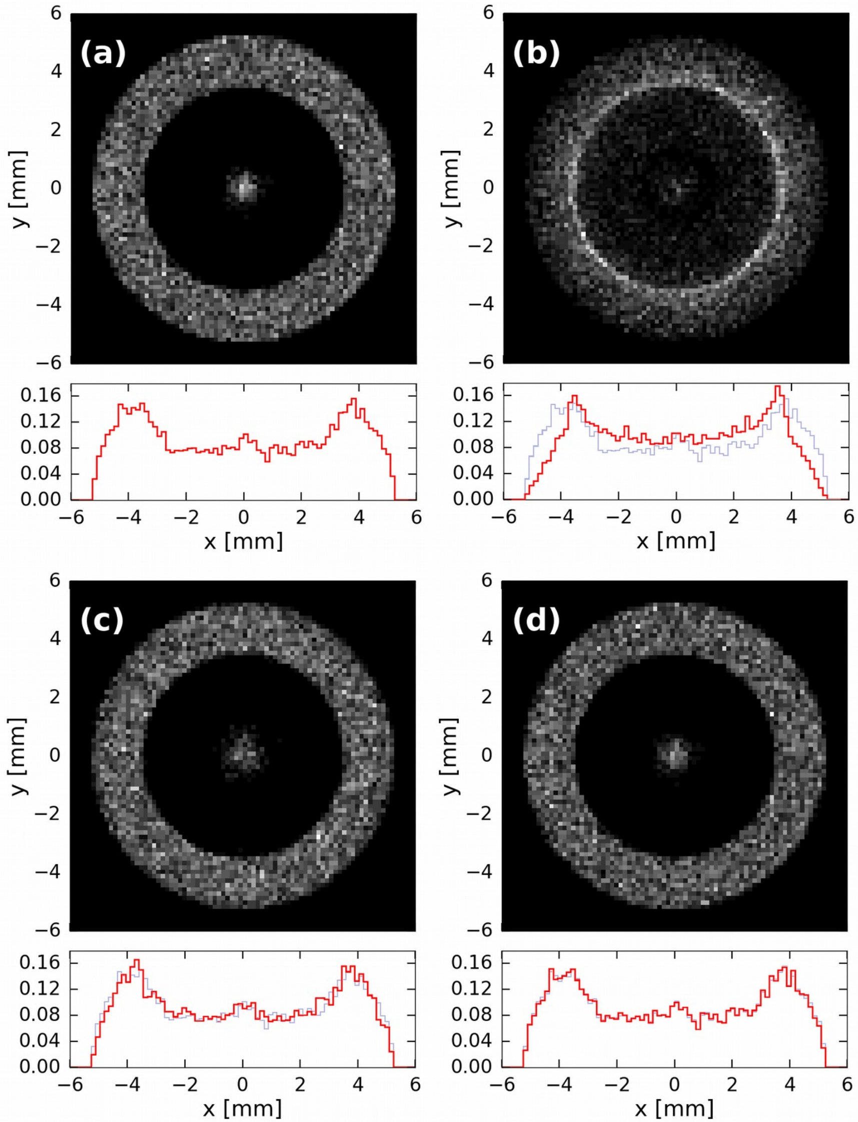

2D and 1D histograms of the detected photons assuming **ideal gas curtain and optics with unit magnification**. The bin size is 0.15 mm. The 1D histograms are normalized.

(a) No distorsions
(b) N_2^+, τ_{BIF} = 60 ns
(c) Ne^+, τ_{BIF} = 11 ns
(d) Ar^+, τ_{BIF} = 9 ns

The 1D histogram from (a) is reproduced in grey in all the others.

Simulation parameters

B_{sol} = 1 T
I_e = 5 A
D_e = 10.5 mm
d_e = 7 mm
$\langle I_p \rangle$ = 1 A
σ_{tp} = 0.3 mm
$4 \cdot \sigma_{lp}$ = 1.01 ns
$N_\gamma^e \approx 12500$
$N_\gamma^p \approx 250$

Such simulations should be performed with a realistic gas curtain too for a better reproduction of the image to be expected.

Influence of curtain thickness: Assumptions

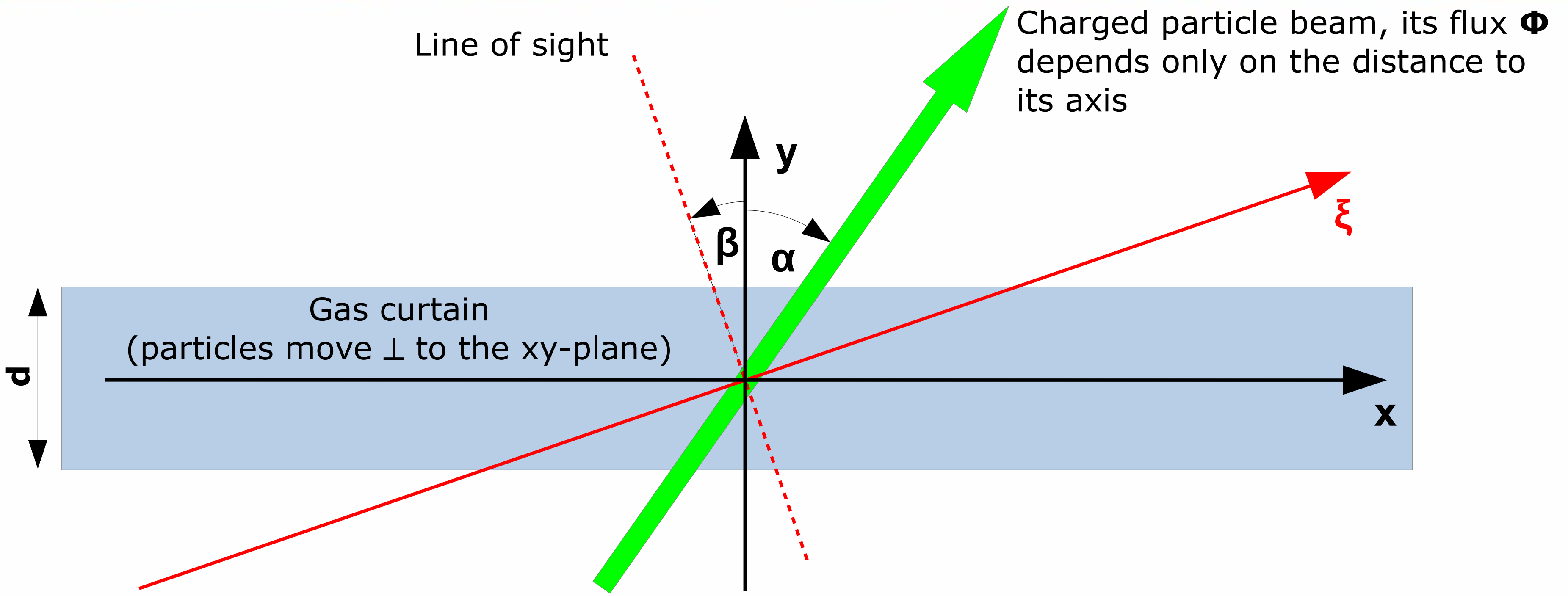

- Gas curtain's density **ρ** depends only on **y**
- Gas curtain's refractive index is 1
- Gas curtain extends from **y** = -d/2 to **y** = d/2
- 1D detector parallel to the **ξ** axis
- Ideal optics placed practically at infinity
- Practically infinite depth of field
- 0 ≤ **β** < 90° **(presently 45°)**
- -90° < **α** < 90° **(presently 45°)**

$$I(\xi) \propto \int_{-d/2}^{d/2} \rho(y) \cdot \phi\left(\xi \cdot \frac{\cos(\alpha)}{\cos(\beta)} - \frac{\sin(\alpha+\beta)}{\cos(\beta)} \cdot y\right) dy$$

Gaussian beam & homogeneous gas curtain

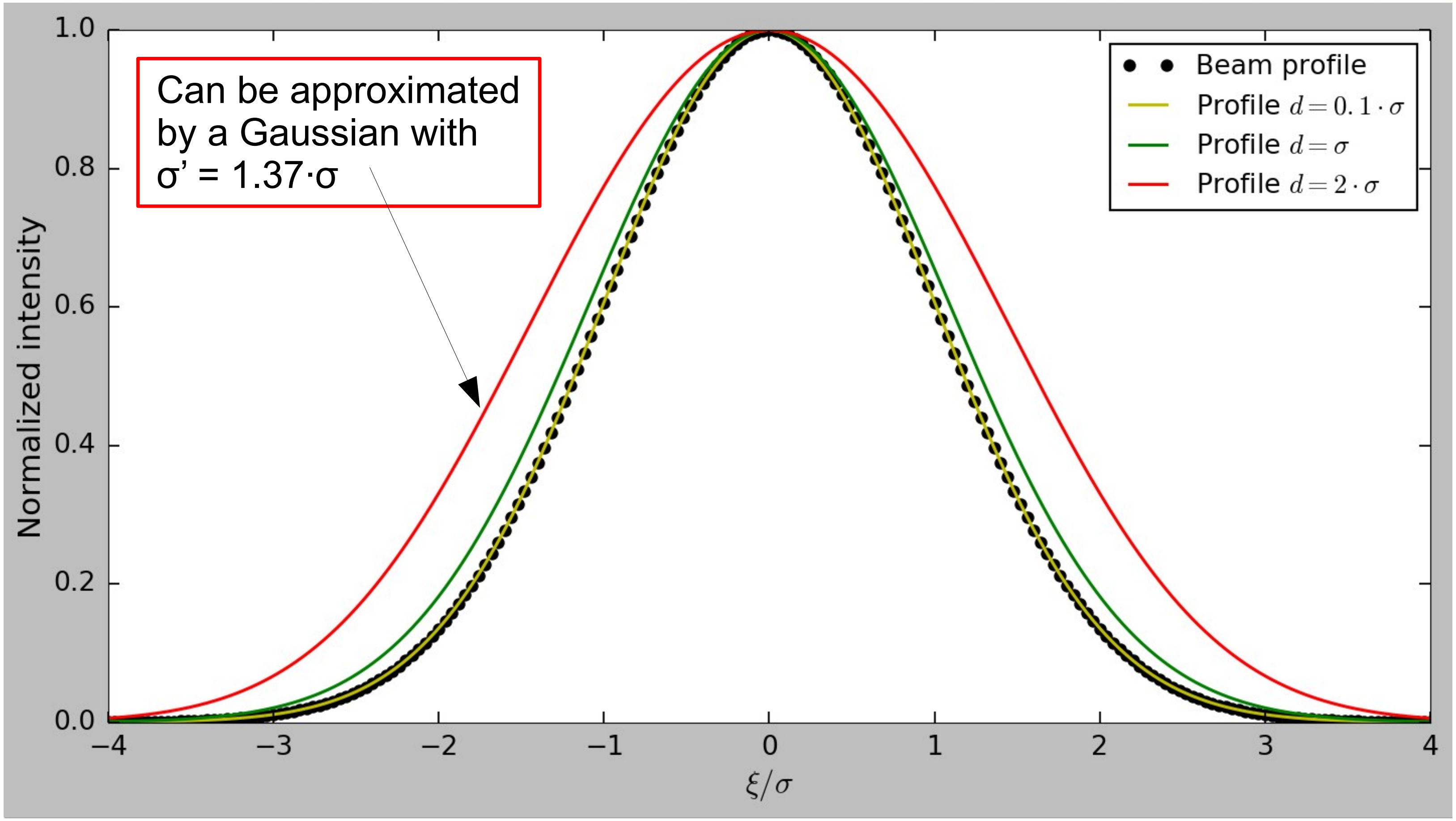

Line of sight and beam axis are perpendicular to each other, moreover α = β = 45°
The charged particle beam has a Gaussian profile with standard deviation **σ**, three gas curtain thicknesses **d** are considered: 0.1·**σ**, **σ** and 2·**σ**.

Gaussian beam & parabolic gas curtain profile

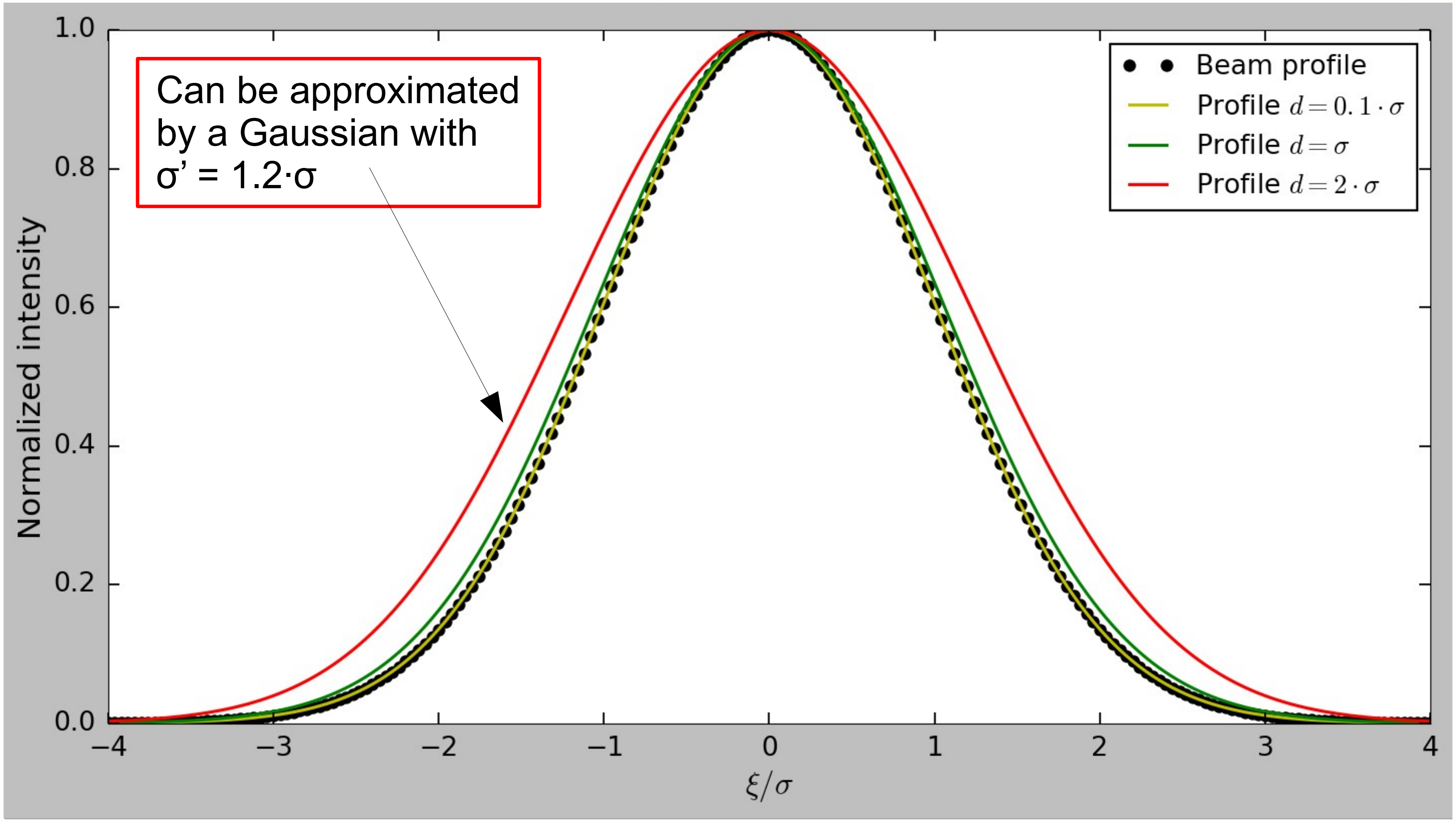

Line of sight and beam axis are perpendicular to each other, moreover α = β = 45°
The charged particle beam has a Gaussian profile with standard deviation **σ**, three gas curtain thicknesses **d** are considered: 0.1·**σ**, **σ** and 2·**σ**.

Gaussian beam & parabolic gas curtain profile

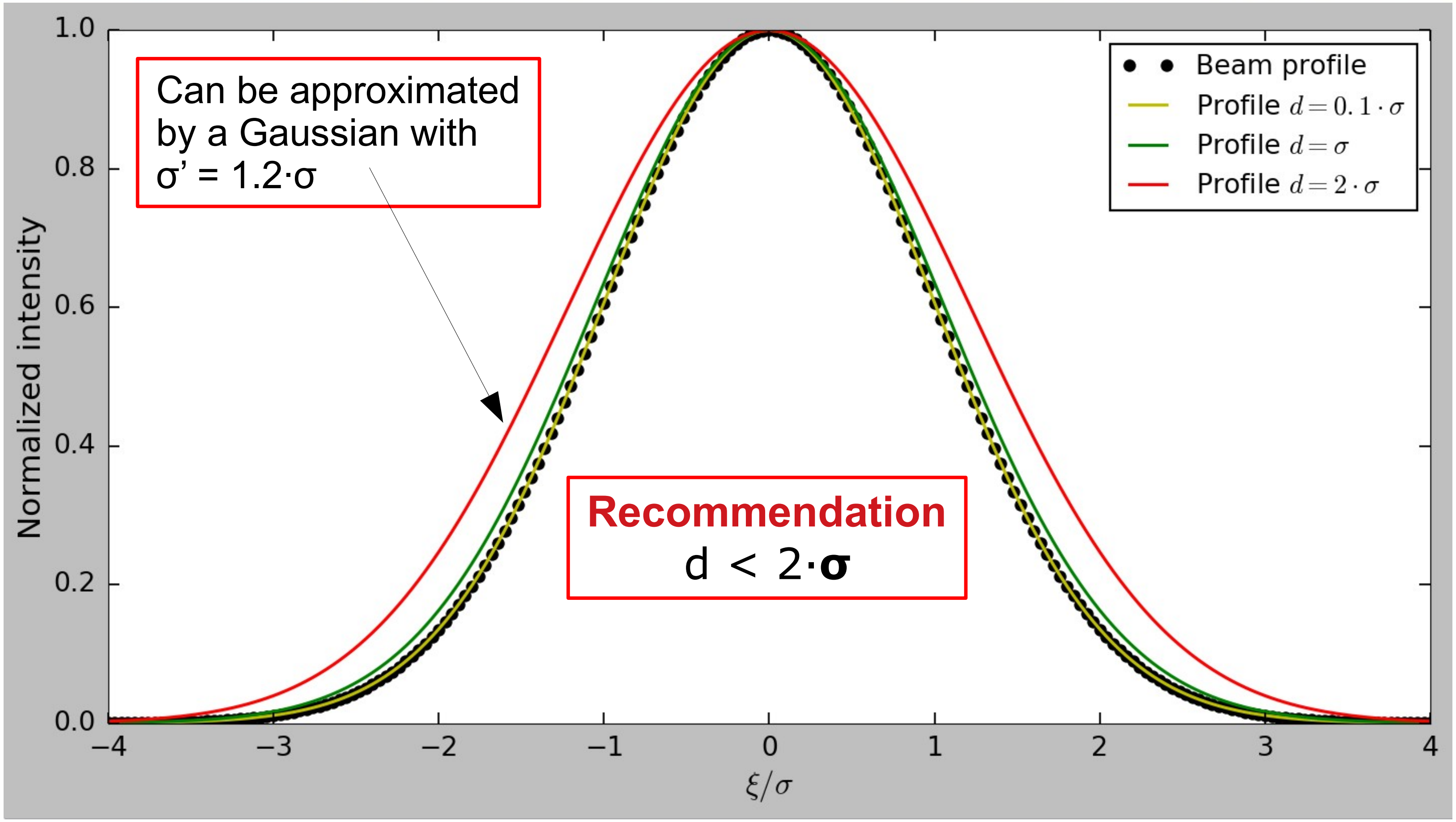

Line of sight and beam axis are perpendicular to each other, moreover α = β = 45°
The charged particle beam has a Gaussian profile with standard deviation **σ**, three gas curtain thicknesses **d** are considered: 0.1·**σ**, **σ** and 2·**σ**.

Possible show stoppers

- **secondary, low energy electrons and ions** accumulating in the e-lens may generate a strong background due to the usually high fluorescence cross sections at low energies
- **gas curtain density and thickness** since thin curtains are needed for good spatial resolution the gas density has to be maximized; in case of a too thick curtain image blurr and decreased resolution are expected
- **strong electromagnetic fields** in case of ions as emitters, however recent simulations show that in the region where the BGC based diagnostic will be performed this effect should be negligible for Ar^+ and Ne^+
- **energy distribution of the electrons** within the main hollow beam since cross sections are energy dependent.
- **synchrotron radiation**
- **high energy radiation background**
- **cluster formation within the gas jet** especially in case of Ar

Conclusion

There is no clear winner yet, but Ne emitting at 584.5 nm might be finally the best choice, especially if a detector (camera) can be identified which has good – at least 20% – efficiency at this wavelength and is capable of single photon detection.

Ar^{+} may however lead to a stronger signal, especially if detection can be extended over the whole wavelength range from 400 to 500 nm. But Ar is expected to be prone to clustering.

An alternative technical solution may be an emCCD camera, classical or back illuminated. But its radiation hardness is questionable and it is an expensive monolitic device which if broken has to be replaced as a whole.